Available online at www.sciencedirect.com
SCIENCE DIRECT®
Journal of Magnetic Resonance 170 (2004) 127–135
JMR Journal of Magnetic Resonance
www.elsevier.com/locate/jmr

Direct-detected rapid-scan EPR at 250 MHz

James W. Stoner, Dennis Szymanski, Sandra S. Eaton,* Richard W. Quine, George A. Rinard, and Gareth R. Eaton

Department of Chemistry and Biochemistry and Department of Engineering, University of Denver, Denver, CO 80208, USA

Received 22 April 2004; revised 13 June 2004
Available online 6 July 2004

Abstract

EPR spectra at 250 MHz for a single crystal of lithium phthalocyanine (LiPc) in the absence of oxygen and for a deoxygenated aqueous solution of a Nycomed triarylmethyl (trityl-CD_3) radical were obtained at scan rates between 1.3×10^3 and 3.4×10^5 G/s. These scan rates are rapid relative to the reciprocals of the electron spin relaxation times (LiPc: $T_1 = 3.5\,\mu s$ and $T_2 = 2.5\,\mu s$; trityl: $T_1 = 12\,\mu s$ and $T_2 = 11.5\,\mu s$) and cause characteristic oscillations in the direct-detected absorption spectra. For a given scan rate, shorter values of T_2 and increased inhomogeneous broadening cause less deep oscillations that damp out more quickly than for longer T_2. There is excellent agreement between experimental and calculated lineshapes and signal amplitudes as a function of radiofrequency magnetic field (B_1) and scan rate. When B_1 is adjusted for maximum signal amplitude as a function of scan rate, signal intensity for constant number of scans is enhanced by up to a factor of three relative to slow scans. The number of scans that can be averaged in a defined period of time is proportional to the scan rate, which further enhances signal amplitude per unit time. Longer relaxation times cause the maximum signal intensity to occur at slower scan rates. These experiments provide the first systematic characterization of direct-detected rapid-scan EPR signals.

Keywords: Rapid-scan; EPR; Direct-detection; Trityl; Lithium phthalocyanine; 250 MHz EPR

1. Introduction

Early in the development of NMR transient effects, called "wiggles," were observed after the magnetic field passed through resonance in a time that was short relative to T_1 and T_2 [1,2]. Since inhomogeneity over the sample causes the oscillations to damp out more rapidly, this effect was used in CW NMR to guide shimming the magnetic field to maximum homogeneity. It was shown that the undistorted NMR lineshapes could be recovered from rapid-scan spectra by deconvolution using either a standard experimental spectrum [3–5] or a computed spectrum [6–8]. This technique was called "Correlation NMR Spectroscopy," or "Rapid-Scan Fourier Transform NMR Spectroscopy." Rapid-scan NMR achieved almost as high a signal-to-noise, per unit time, for proton spectra of simple organic molecules in fluid solution as could be achieved by pulsed FT-NMR. For example, with T_1 equal to 1 s and a full spectral scan in four T_1, correlation spectroscopy was only 35% less sensitive than a pulsed FT experiment acquired with a period of three T_2 [9]. Rapid scan looked very promising for NMR in the early 1970s, but was soon eclipsed by FT-NMR due to the wide range of pulse sequences that became available [9].

Traditionally most EPR spectra are run in the linear-response slow-scan regime, in which the signal lineshape is not sensitive to spin relaxation times unless partially power saturated. At the other extreme are pulse experiments in which the microwaves cause large changes in the orientation of the net magnetization vector and produce spin responses that are strongly dependent on relaxation times. In between these two extremes there is a variety of non-linear responses that are collectively called "passage effects." Bloch first described passage effects for NMR signals [10]. The initial observation of adiabatic rapid passage EPR by Portis [11] was followed by papers by Weger [12], Hyde [13,14], and Mailer [15],

* Corresponding author. Fax: 1-303-871-2254.
E-mail address: sandra.eaton@nsm.du.edu (S.S. Eaton).

1090-7807/$ - see front matter © 2004 Elsevier Inc. All rights reserved.
doi:10.1016/j.jmr.2004.06.008

among others, that demonstrated the importance of passage effects in EPR spectra. Since the observed signals depend upon the relative values of magnetic field sweep rate (dB_0/dt), relaxation times (T_1, T_2), microwave or RF magnetic field B_1, and magnetic field modulation frequency (ω_m) and amplitude (B_m), terminology evolved to identify particular regimes [12,15,16]. The term "rapid" refers to the regime in which $B_1/[(dB_0/dt)(T_1T_2)^{0.5}] < 1$ [12], which is the regime in which the studies reported here were performed.

Most prior studies of EPR passage effects were performed using phase-sensitive detection at the magnetic field modulation frequency. The phase relationship between the EPR signal and the modulation is central, for example, to the technique of saturation transfer EPR [17,18]. By contrast, the spectra reported in this paper were obtained by direct detection at the resonance frequency, as is used in pulsed EPR. By using direct detection the EPR absorption signal is obtained, instead of the traditional first-derivative signal. In an imaging experiment the magnetic field gradient broadens the EPR signal. The amplitude of the absorption signal decreases proportional to the signal width, whereas the amplitude of the first derivative signal decreases proportional to the square of the signal width. Thus, for constant noise, the degradation of signal-to-noise with increasing gradient is less when the absorption signal is detected than when the first-derivative is detected. This potential advantage for imaging experiments provides a strong incentive for developing methodology to record EPR absorption signals. Also, most prior studies of rapid passage signals were performed in the regime called "adiabatic" where the signal is partially saturated and the scans are characterized by $(\omega_m H_m/\gamma B_1^2) \ll 1$ or $(dB_0/dt)/(\gamma B_1^2) \ll 1$ [12]. Most of the signals reported in this study were recorded under non-adiabatic conditions where there is little or no saturation of the signal.

The true slow-scan EPR or NMR lineshape is observed when

$$\frac{dB_0}{dt} \ll \gamma(\delta B_0)^2, \tag{1}$$

where δB_0 is the relaxation-determined linewidth expressed in magnetic field units [2]. If magnetic field modulation is large relative to linewidth, it is possible to pass through a line very rapidly. For example, for a 1 G peak-to-peak modulation amplitude at 100 kHz the magnetic field at the point of maximum slope of the sinusoidal scan changes at the rate $\pi \times 10^5$ G/s ($2\pi \times$ scan frequency $\times$ peak-to-peak scan width/2). If we define

$$\boldsymbol{a} = |\gamma|\left(\frac{dB_0}{dt}\right) \tag{2}$$

then oscillations in the signal response are seen if $\boldsymbol{a}^{1/2}T_2 \geqslant 1$ [2]. Rengen et al. [19] considered the rates of magnetic field scan at which passage effects and detector filter bandwidth effects would distort a rapid-scan EPR signal. The "wiggles" (oscillations) following a rapid-scan EPR signal were observed by Czoch et al. [20].

The experiments reported in this paper were performed at 250 MHz because of our interest in developing methods for in vivo spectroscopy and imaging and the need to exploit approaches for enhancing signal intensity at these low frequencies. The trityl radical and LiPc were selected for study because of their potential for use in in vivo oximetry [21,22]. For samples with long relaxation times, as are observed for these species in the absence of oxygen, rapid-scan spectra are predicted to have enhanced intensities compared with slow-scan spectra. To define parameters that optimize rapid-scan signals, spectra were obtained as a function of scan rate and B_1 and compared with simulations.

2. Experimental methods

2.1. Samples

Lithium phthalocyanine (LiPc) prepared electrochemically following the literature procedures [23,24] was provided by Prof. Swartz, Dartmouth University. Well-shaped needles were selected, placed in 4 mm O.D. quartz tubes, evacuated overnight on a high vacuum line, and the tubes were flame sealed. Solutions (0.2 mM) of Nycomed trityl-CD_3 (methyl tris(8-carboxy-2,2,6,6-tetramethyl (d_3)-benzo[1,2-d:4,5-d']bis(1,3)dithiol-4-yl)-tri potassium salt) [22] in water in 4 mm O.D. quartz tubes were bubbled extensively with N_2 gas to remove oxygen and then flame sealed.

2.2. Spectroscopy

Spectra at 250 MHz were obtained on a locally designed and constructed spectrometer [25] with a 40 cm diameter air-core magnet and a Bruker Elexsys E540 console. Rapid magnetic field scans were generated with the modulation driver in the Bruker console and 7-in. diameter Helmholtz coils. The scan widths were calibrated using the peak-to-peak separations of LiPc signals in slow scans recorded with phase sensitive detection. Scan frequencies were between 1 and 50 kHz and scan widths were 0.4–2.0 G. Scans are labeled with the maximum rate, which occurs at the center of the scan. Since the magnetic field scans are sinusoidal, the rates decrease toward the extremes of the scans. The 3 dB cut-off of the high-pass filter in the amplification stage of the signal channel in the bridge was decreased from 677 [25] to 16 Hz to decrease the impact of the filter on spectra obtained at scan frequencies below 5 kHz. Low-pass filters in the bridge signal channel can be selected to have either 1 or 5 MHz 3 dB bandwidth. The

1 MHz bandwidth was used for scans with maximum rates less than about 5×10^4 G/s, and the 5 MHz bandwidth was needed for faster scans. The incident power on the resonator at 0 dB is 43 mW. Rapid-scan data were acquired in quadrature using the pulse signal pathway in the bridge [25] and digitized with the Bruker SpecJet. Acquisition of quadrature data permitted optimization of signal phasing by post-processing. Signal amplitude was defined as the amplitude above the baseline, and does not include oscillations that go below the baseline.

The data shown in the figures of this paper were obtained with a 5-turn helical resonator constructed from no. 16 copper wire with an internal diameter of about 4.3 mm, a wire-wound shield that is about 28 mm in diameter and 25 mm high, and series-capacitive coupling of the resonator to the transmission line. The resonating capacitor is a copper disk approximately 12 mm in diameter, positioned approximately 0.15 mm from the end of the shield by a Teflon spacer with a hole, which is concentric with the capacitor disk and about 10 mm in diameter. One end of the resonator coil is connected to the same end of the shield and the other end to the capacitor disk. The Q of this resonator, measured with an HP 8753D network analyzer, was about 160. With the sample in the resonator, the resonant frequency was 252 MHz for the LiPc sample and 250 MHz for the aqueous trityl-CD_3 sample. To test the impact of resonator Q on the rapid-scan lineshapes representative data were recorded with two other resonators. The Q of a tellurium–copper loop-gap resonator with a 26 mm loop was reduced to 280 with conducting plastic film. The other resonator consisted of two 6-turn 4.3-mm helical loops of no. 14 copper wire. The loops were in parallel, in a reentrant configuration, and the parallel combination was resonated with a homemade capacitor with Teflon dielectric. The Q of this resonator was reduced to 65 by placing a 3 kΩ, 1/8 watt resistor in parallel with the coils. This resonator was used with and without a 0.001 in. thick brass-foil shield. This resonator could be used without the shield because of its reentrant construction, but was subject to excessive pick-up and hand-waving effects.

2.3. Simulation of rapid-scan spectra

Simulations were performed by numerical integration of the rotating-frame representation of the Bloch equations including magnetic field scan as shown in the expressions in Eq. (3) [26]

$$\begin{aligned}
\frac{dM_u}{dt} &= \frac{-M_u}{T_2} - (\Delta\omega + \Omega_m \cos(\omega_m t))M_v, \\
\frac{dM_v}{dt} &= (\Delta\omega + \Omega_m \cos(\omega_m t))M_u - \frac{M_v}{T_2} - \gamma B_1 M_z, \\
\frac{dM_z}{dt} &= \frac{M_0}{T_1} + \gamma B_1 M_v - \frac{M_z}{T_1},
\end{aligned} \tag{3}$$

where γ, the electron magnetogyric ratio is 1.7608×10^7 rad s^{-1} G^{-1}; $\Delta\omega = \omega_0 - \omega$ is the offset of a spin packet from the center of the scan in angular frequency; Ω_m is the amplitude of the field scan in angular units and equals 0.5 γB_m, where B_m is the peak-to-peak scan amplitude in gauss; ν_m is the scan frequency in Hz; $\omega_m = 2\pi\nu_m$ is the angular scan frequency; and B_1 is the RF magnetic field in gauss (peak-to-peak). The time evolution of the magnetization for a spin packet was evaluated using fourth-order Runge–Kutta numerical integration [27] performed at 20,000 to 40,000 points per field scan cycle. For the relaxation times of the LiPc and trityl-CD_3 samples, calculation for 8 cycles was sufficient to reach a steady-state signal. Simulations were calculated with a program written in Compaq Visual Fortran 6.5. A typical calculation for a trityl-CD_3 signal took about 5 s on a 3.0 GHz Pentium 4 PC.

For a single spin-packet the simulated signal at slow scan rates is a Lorentzian with T_2-determined linewidth. The experimental lineshapes at scan rates that are too slow to exhibit oscillations are not purely Lorentzian because of magnetic field inhomogeneity over the finite dimensions of the sample and unresolved nuclear hyperfine splittings (trityl) or incomplete exchange narrowing (LiPc). The lineshapes were modeled as the sum of contributions from multiple T_2-determined spin packets with differing offsets from the center of the signal. The weightings of the spin packets in the distribution were calculated using an approximation for a Voigt function Eq.(4) [28],

$$\mathrm{Wgt}_i = F \Bigg/ \left[1 + \left(\frac{dx_i}{\mathrm{broad}}\right)^2\right] + (1-F)\exp\left[-0.693\left(\frac{dx_i}{\mathrm{broad}}\right)^2\right], \tag{4}$$

where Wgt_i is the weighting for the ith spin packet, F is the fraction Lorentzian for the distribution, broad is the half-width at half height of the distribution, and dx_i is the offset for the ith spin packet. Spin packets were spaced at equal intervals in magnetic field extending for six times broad. The parameters F and broad were adjusted to fit the spectra obtained at a scan rate of 1.3×10^3 G/s, where oscillations were not observed. For LiPc broad = 3 mG and $F = 0.05$, consistent with the nearly Lorentzian experimental lineshape. For trityl-CD_3 broad = 14.5 mG and $F = 0.15$, consistent with an experimental lineshape intermediate between Gaussian and Lorentzian. The ^{13}C sidebands for the trityl-CD_3 signal were included with a hyperfine splitting of 0.166 G and intensity of each sideband of 0.033 (6 equivalent carbons) relative to the center ($I = 0$) line. To produce a smooth lineshape, contributions from 15 or 45 spin packets were summed for LiPc or trityl-CD_3, respectively.

Due to the triggering of the SpecJet digitizer, the timing of the first point in the experimental array is at an

arbitrary (but reproducible) point in the sinusoidal scan cycle. The experimental and calculated shapes were overlaid by manually aligning the peaks in the experimental and calculated arrays. The cosine relationship between time and magnetic field in the calculated array was used to convert the axes for the experimental and calculated data that are linear in time to a scale that is linear in gauss.

The Q for a resonator is defined as ω/BW, where BW is the 3 dB bandwidth of the resonator. At 250 MHz a Q of 160 corresponds to BW ~1.6 MHz which has a significant impact on the rapid-scan lineshapes for the LiPc or trityl-CD_3 signals at scan rates greater than about 5×10^4 G/s. To match the experimental data filtering of the simulated signal was performed in the time-domain by convolution or in the Fourier domain as a multiplication. The requisite filter functions in the two domains are:

$$f(t) = \exp(-t\pi v_0/Q) \quad \text{or}$$
$$F(\omega) = \frac{1 - i\omega Q/\pi v_0}{1 + \omega^2 Q^2/(\pi v_0)^2}, \tag{5}$$

where the independent variables in the two domains are t or ω, respectively, and v_0 is the resonant frequency. The filtering in the signal channel of the bridge was approximated as a simple RC circuit and the corresponding functions in the two domains are:

$$f(t) = \exp(-t2\pi\,\text{bwidth}) \quad \text{or}$$
$$F(\omega) = \frac{1 - i\omega/(2\pi\,\text{bwidth})}{1 + \omega^2/(2\pi\,\text{bwidth})^2}, \tag{6}$$

where bwidth is the 3 dB bandwidth of the filter. Filtering in the time or frequency domain gave the same lineshapes. In the simulations resonator Q and the 3 dB bandwidth of the filter in the bridge were fixed at the measured values.

At higher scan rates, small adjustments in scan widths were made to match the period of the oscillations after passage through the signals. The period of these oscillations is more sensitive to scan rate than the precision with which we can measure the peak-to-peak linewidths in the slow-scan modulation amplitude calibrations. T_1 was fixed at the value measured by inversion recovery: 12 μs for trityl-CD_3 [29] and 3.5 μs for LiPc. T_2 was adjusted to fit the decay of the oscillations and the resulting values were in good agreement with time constants measured by two-pulse spin echo: 11.5 μs for trityl-CD_3 [29] and 2.5 μs for LiPc.

3. Results

3.1. LiPc

The traditional slow-scan phase-sensitive detected spectrum of LiPc is a single line with first derivative peak-to-peak linewidth of 26 mG. This linewidth is in good agreement with the spin packet linewidth expected for $T_2 = 2.5$ μs measured by two-pulse spin-echo. The approximately Lorentzian lineshape also is consistent with the assignment of the linewidth as relaxation determined. This linewidth is so narrow that if spectra are recorded with the traditional 100 kHz magnetic field modulation and phase sensitive detection at the modulation frequency, modulation sidebands cause broadening of the line. Therefore, the slow-scan CW spectra were recorded with 5 kHz magnetic field modulation. The first integral of the derivative CW spectrum (Fig. 1B) has a full width at half-height of 44 mG. The ratio of the full width at half-height of the absorption

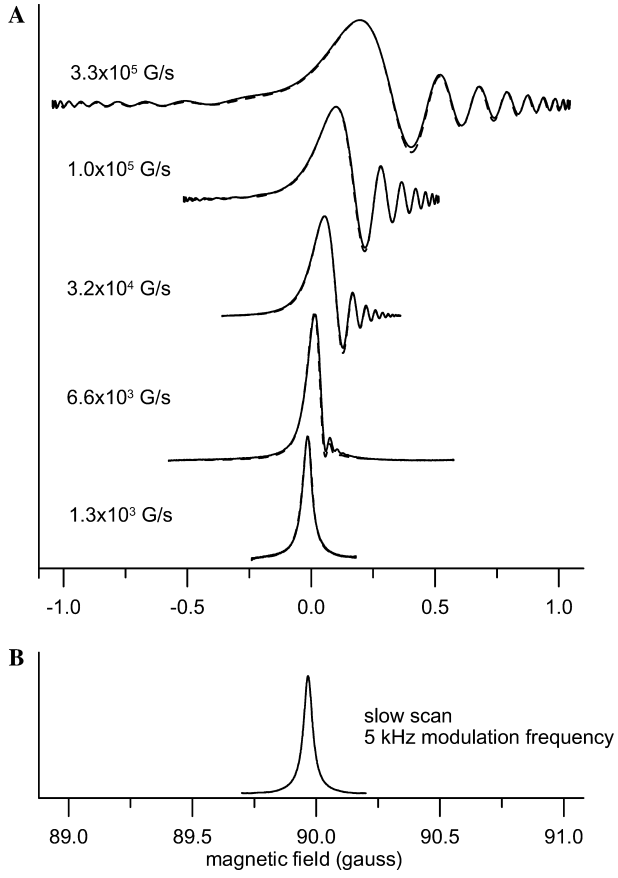

Fig. 1. EPR spectra of LiPc at about 252 MHz. (A) Rapid-scan spectra obtained at the scan rates shown. The x-axis is the offset from resonance (in gauss) and the spectral widths of the traces are the scan widths. The direction of the field scan was left-to-right in each trace. The number of scans for each scan rate was selected to give a total signal acquisition time of 84 s. The y-axis scales are arbitrary. The values of B_1, selected to be a factor of two below the values that gave the maximum signal intensity, were: 4.6×10^{-2} G at 3.3×10^5 G/s, 2.6×10^{-2} G at 1.0×10^5 G/s, 1.8×10^{-2} G at 3.2×10^4 G/s, 1.15×10^{-2} at 6.6×10^3 G/s, and 4.6×10^{-3} G at 1.3×10^3 G/s. Simulated spectra calculated using numerical integration of the Bloch equations (Eq. (3)) and the parameters given in the text are shown as dashed lines, overlaid on the experimental data. (B) First integral of conventional slow-scan spectrum obtained with 5 kHz modulation frequency, modulation amplitude of 10 mG, $B_1 = 4.6 \times 10^{-3}$ G, 84 s scan, 252.07 MHz.

spectrum to the first derivative peak-to-peak linewidth (44/26 = 1.7) is consistent with expectations for a Lorentzian line [30].

Rapid-scan spectra at 252 MHz of LiPc are shown in Fig. 1A for a range of more than 100 in field scan rate. Spectra are labeled with the scan rate at the center of the scan, which is the resonant field for LiPc. The scan rate slows towards the extremes of the scans. At a scan rate of 1.3×10^3 G/s the rapid-scan signal is superimposable on the first-integral of the conventional phase-sensitive-detected CW signal (Fig. 1B). Simulation of the first-derivative signal (Fig. 1B) or of the rapid-scan signals required inclusion of a small inhomogeneous broadening. Inhomogeneous broadening was included in the rapid-scan simulation by summing the contributions from spin packets that differed in offset from the center of the signal. As the scan rate is increased, an oscillation appears on the trailing edge of the signal. When the scan is rapid relative to T_2 the net magnetization does not relax during the time that the spin is in resonance. As the signal is traversed, a significant component of magnetization is created in the x–y plane. This component precesses in the x–y plane and a signal analogous to an FID is detected. However, unlike a pulse experiment that creates and detects an FID at constant magnetic field, the magnetic field is constantly changing in the rapid-scan experiment, which changes the precession frequency. As the field moves off resonance, the offset between the magnetic field and the resonant field increases and the interval between the peaks of the oscillation decreases (Fig. 1A). The amplitude of the oscillation increases as the scan rate increases. For a magnetic field scan rate of 6.6×10^3 G/s the value of $\boldsymbol{a} = \gamma \mathrm{d}B_0/\mathrm{d}t$ (Eq. (2)) is 1.16×10^{11} and $\boldsymbol{a}^{1/2}T_2 = 0.85$. Thus, the onset of oscillations at this scan rate is consistent with the expectation that they will be observed when $\boldsymbol{a}^{1/2}T_2 \geqslant 1$ [2]. The oscillations on the left side of the scan at 3.3×10^5 G/s (Fig. 1A) are due to the previous traverse of the signal.

At the faster scan rates the magnetic field has moved further from resonance during the time that the oscillation persists, so when the signal is displayed on a magnetic field axis (as in Fig. 1A) the signal is broadened. The broadening of the signal increases with increasing scan rate. For the five scan rates shown in Fig. 1A the full widths at half height for the signals are: 44 mG (1.3×10^3 G/s), 62 mG (6.6×10^3 G/s), 100 mG (3.2×10^4 G/s), 148 mG (1.0×10^5 G/s), and 260 mG (3.3×10^5 G/s). Thus, although the broadening is modest at relatively low scan rates, it becomes very large at higher scan rates. The changes in lineshape as a function of scan rate agree well with the simulations (Fig. 1A).

If the RF power (and therefore B_1) is held constant at a value that is well below saturation at a scan rate of 1.3×10^3 G/s and the scan rate is increased, the amplitude of the rapid-scan signal decreases (Fig. 2) because

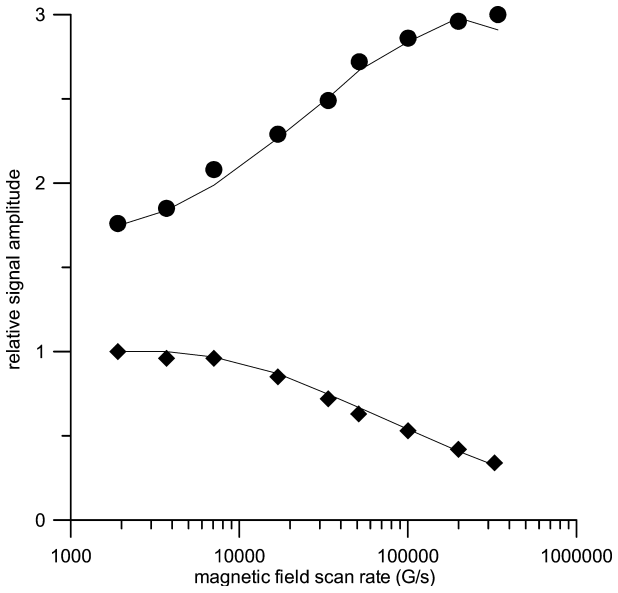

Fig. 2. Relative intensities for the LiPc signal at the center of the scan as a function of scan rate at constant RF B_1 of 6.5×10^{-3} G (◆) and at the B_1 that gave the maximum signal amplitude (●). The number of scans was held constant. The relative signal amplitudes were scaled to 1.0 for the signal at constant B_1 of 6.5×10^{-3} G collected at the scan rate of 1.3×10^3 G/s (scan width of 0.42 G and scan frequency of 1 kHz). The solid lines connect points that were calculated by numerical integration of the Bloch equations (Eq. (3)) using the parameters for LiPc and the experimental scan widths and frequencies.

the total energy deposited in the spin system decreases with increasing scan rate. However, if the RF B_1 at each scan rate is increased to produce the maximum signal amplitude, then the amplitude at higher scan rates is about 60% larger than at 1.3×10^3 G/s. There is excellent agreement between the experimental and calculated signal amplitudes for the two cases-constant B_1 and B_1 selected for maximum intensity (Fig. 2). The signal intensities in Fig. 2 are for constant number of scans. When the increase in number of scans that can be acquired per unit time at faster scan rates is taken into account, the signal enhancement with increasing scan rate is much greater. For example, provided that the digitizer can respond to every trigger, a scan rate of 10 kHz and scan width of 1.0 G (3.1×10^4 G/s) would acquire 10 times as many scans per unit time as a scan rate of 1 kHz and scan width of 1.0 G (3.1×10^3 G/s). The RF B_1 required to produce the maximum signal amplitude as scan rate is increased is shown in Fig. 3. Based upon the comparison between calculated B_1 and the power incident on the resonator that was required to give the maximum experimental signal amplitude, $B_1 = (5.5 \pm 0.5)\sqrt{P(\mathrm{watt})}$ for the helical coil resonator.

The spectra shown in Fig. 1A were obtained at B_1 that is a factor of two less than the values that gave maximum signal amplitude. At these B_1 values the signal amplitude is about 75% of the maximum value and the linewidths are within a few percent of the values

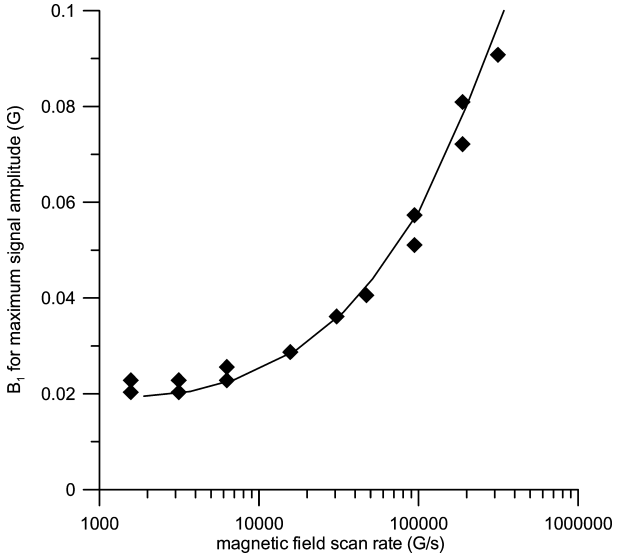

Fig. 3. Radiofrequency magnetic field (B_1) required to obtain the maximum signal amplitude for LiPc at the center of the scan as a function of scan rate. Data are shown for two replicate data sets (◆). The solid line connects points that were calculated by numerical integration of the Bloch equations using the parameters for LiPc and the experimental scan widths and frequencies.

observed in the regime where signal increases linearly with B_1. At the B_1 that gave the maximum signal amplitude the linewidths were about 20% greater than in the linear response regime.

3.2. Trityl-CD_3

The slow-scan phase-sensitive detected spectrum of trityl-CD_3 in water (Fig. 4B) has a major peak plus two ^{13}C sidebands that are assigned to six equivalent carbons on the three aryl rings [22]. The splitting between the two sidebands is 0.166 G. In the first-derivative display the peak-to-peak width of the center line is 24 mG which is substantially broader than the 6.0 mG spin packet width predicted for $T_2 = 11.5\,\mu s$ [29]. The additional broadening is attributed to unresolved deuterium and ^{13}C hyperfine splitting and to magnetic field inhomogeneity over the dimensions of the sample. The first integral of the CW spectrum shown in Fig. 4B has a full width at half height of 34 mG. The ratio of the full width at half-height of the absorption spectrum to the first derivative peak-to-peak linewidth ($34/24 = 1.4$) is consistent with a lineshape intermediate between Lorentzian and Gaussian [30] due to the inhomogeneous broadening of the relaxation-determined lineshape.

Rapid-scan spectra at 250 MHz for trityl-CD_3 are shown in Fig. 4A. At a scan rate of 1.3×10^3 G/s the rapid-scan spectrum is indistinguishable from the first integral of the slow-scan spectrum (Fig. 4B). The changes in the lineshape for the trityl-CD_3 signal as a function of scan rate are similar to what was observed for LiPc, but

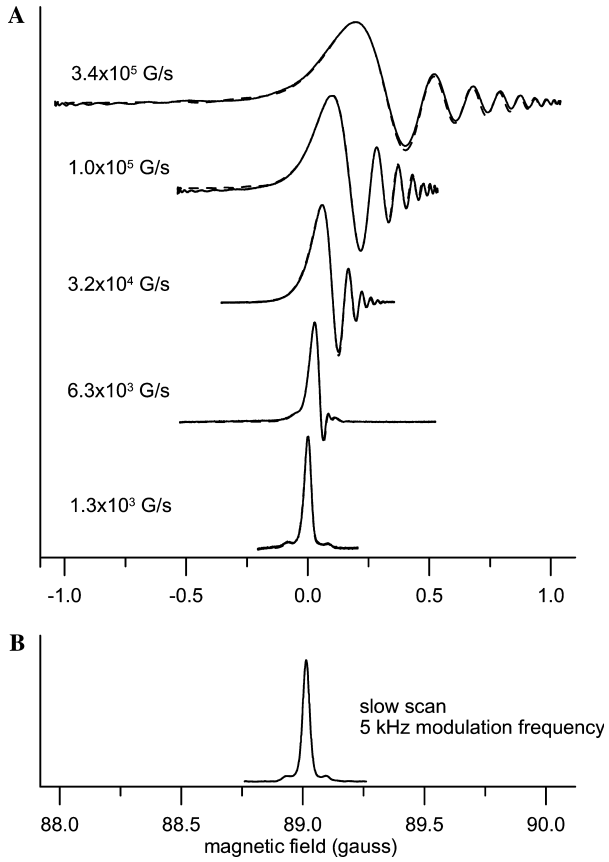

Fig. 4. EPR spectra of trityl-CD_3 at about 250 MHz. (A) Rapid-scan spectra obtained at the scan rates shown beside the traces. The x-axis is the offset from resonance (in gauss) and the widths of the traces are the scan widths. The direction of the field scan was left-to-right in each trace. For each scan rate the number of scans was selected to give a total signal acquisition time of 84 s. The y-axis scales are arbitrary. The values of B_1, selected to be a factor of two below the value that gave the maximum signal intensity, were: 3.3×10^{-2} G at 3.4×10^5 G/s, 1.9×10^{-2} G at 1.0×10^5 G/s, 1.3×10^{-2} G at 3.2×10^4 G/s, 7.3×10^{-3} G at 6.3×10^3 G/s, and 4.6×10^{-3} G at 1.3×10^3 G/s. Simulated spectra calculated using numerical integration of the Bloch equations (Eq. (3)) and the parameters given in the text are shown as dashed lines, overlaid on the experimental data. (B) First integral of conventional slow-scan spectrum obtained with 5 kHz modulation frequency, modulation amplitude of 10 mG, $B_1 = 2.0 \times 10^{-3}$ G, 84 s scan, 249.55 MHz.

with significant differences. At each of the scan rates examined the oscillations were deeper for trityl-CD_3 than for LiPc because of the longer T_2 for trityl-CD_3 ($T_2 = 11.5\,\mu s$) than for LiPc ($T_2 = 2.5\,\mu s$). The inhomogeneous broadening of the trityl-CD_3 signal by unresolved hyperfine splittings and magnetic field inhomogeneity resulted in observation of fewer cycles of the oscillations than would be observed for a single spin-packet with the same T_2. The inhomogeneous broadening of the rapid-scan signal was included in the simulation by summing contributions from spin packets that differed in offset from the center of the signal. As seen for the LiPc signal, the lines broaden as the scan rate increases. The full widths at half height for the signals at

the five scan rates shown in Fig. 4A are: 34 mG (1.3×10^3 G/s), 43 mG (6.3×10^3 G/s), 84 mG (3.2×10^4 G/s), 143 mG (1.0×10^5 G/s), and 245 mG (3.4×10^5 G/s). At scan rates greater than about 1×10^4 G/s the broadening is so large that the ^{13}C hyperfine lines are not readily resolved from the central line.

Resonator Q significantly impacted the damping of the oscillations in signal amplitude at the fastest scan rates. The data shown in Fig. 4A were obtained in a resonator with $Q = 160$. Fewer cycles of the oscillations were observed in a resonator with $Q = 280$ and more cycles were observed in a resonator with $Q = 65$. In addition to the effect of resonator Q, simulation of the spectra required an inhomogeneous broadening contribution that increased with increasing scan rate. For the resonators that were examined, the magnitude of the additional inhomogeneity increased as the penetration of the swept field decreased. Also, the additional inhomogeneity was greater when a brass shield surrounded the resonator than when no shield was present. These observations suggest that the inhomogeneity is due to eddy currents induced in the resonator assemblies by the oscillating fields, which add components to the magnetic field that are non-uniform over the sample. These effects were observed for the trityl-CD_3 sample, but not for the LiPc sample. There are two factors that make the eddy current-induced inhomogeneity more conspicuous for trityl-CD_3 than for LiPc. (1) The trityl-CD_3 sample extends over a much larger region of space than the tiny LiPc crystal so magnetic field inhomogeneities have a greater impact. (2) The relaxation times for the trityl-CD_3 signal are longer than for LiPc so the oscillations are expected to damp out more slowly for trityl-CD_3, which makes them more sensitive to other factors that contribute to decay of the oscillations.

The trityl-CD_3 signals at the same scan rates and scan widths as in Fig. 4A are shown in Fig. 5 using the original data acquisition axis that is linear in time. The labeling highlights the fact that the time for a half-cycle of the field scan decreases as the scan rate increases. The T_1 for trityl-CD_3 in H_2O is 12 μs [29]. The time required for the z-axis spin magnetization to fully relax between times that the magnetic field transverses resonance for the signal is approximately $5T_1$, or 60 μs, although much of the magnetization has relaxed within $3T_1$, or 36 μs.

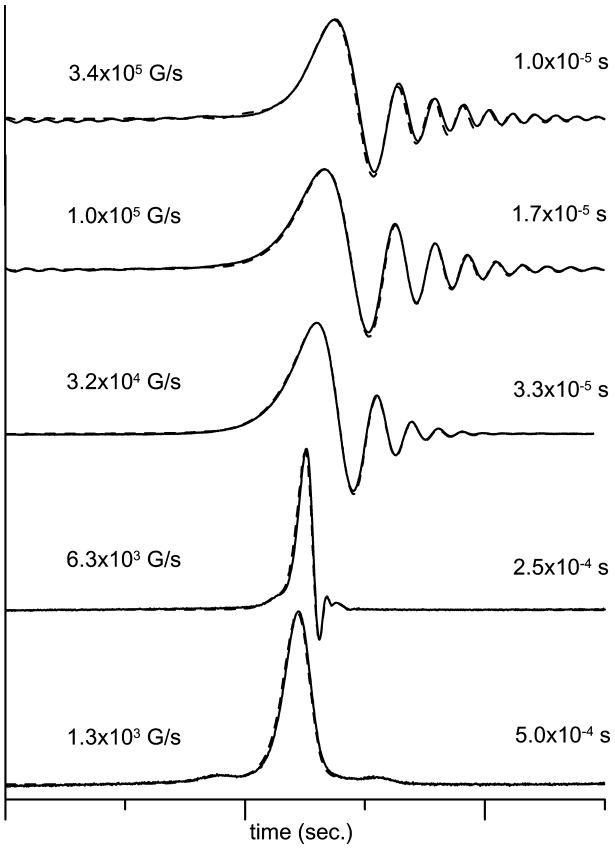

Fig. 5. Time traces of the trityl-CD_3 rapid-scan signal at about 250 MHz. These five traces are the same data as shown in Fig. 4A, but displayed on the original axis that is linear in time. The time interval for each scan rate is shown at the right of the trace. The number of scans was selected to give a total signal acquisition time of 84 s. The y-axis scales are arbitrary. Simulated spectra calculated using numerical integration of the Bloch equations (Eq. (3)) and the parameters given in the text are shown as dashed lines, overlaid on the experimental data.

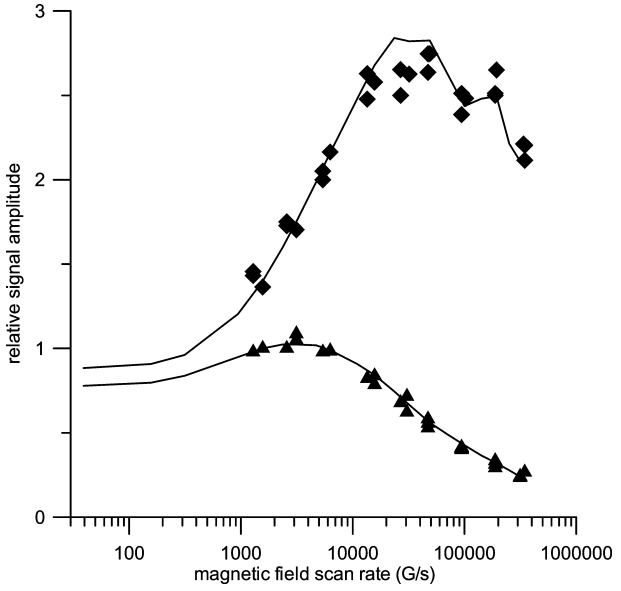

Fig. 6. Relative intensities for the trityl-CD_3 signal at the center of the scan as a function of scan rate at a constant RF B_1 of 4.6×10^{-3} G (▲) and at the B_1 that gave the maximum signal amplitude (◆). The relative signal amplitudes were scaled to 1.0 for the signal at constant B_1 of 4.6×10^{-3} G collected at the scan rate of 1.3×10^3 G/s (scan width of 0.42 G and scan frequency of 1 kHz). Data from three replicate sets are shown. The solid lines connect points that were calculated by numerical integration of the Bloch equations (Eq. (3)) using the parameters for trityl-CD_3 and the experimental scan widths and frequencies. The calculated line for B_1 adjusted to maximize signal is not a smooth curve because scan rates were varied by changing both scan frequency and scan width. At the fastest scan rates, the scan times were short enough that the magnetization does not relax fully between scans through the signal and the signal amplitude depends on scan frequency as well as on scan rate.

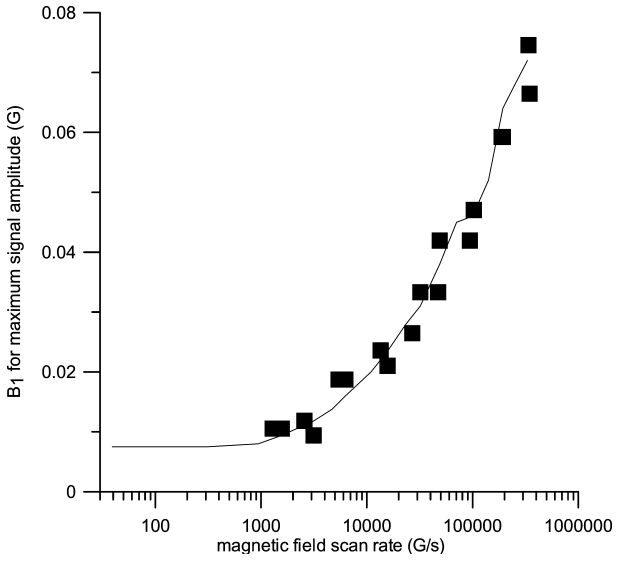

Fig. 7. Radiofrequency magnetic field (B_1) required to obtain the maximum signal amplitude for trityl-CD_3 at the center of the scan as a function of scan rate. Data are shown for three replicate data sets (■). The solid lines connect points that were calculated by numerical integration of the Bloch equations (Eq. (3)) using the parameters for trityl-CD_3 and the experimental scan widths and frequencies. The calculated line is not a smooth curve because scan rates were varied by changing both scan frequency and scan width. At the fastest scan rates, the scan times were short enough that the magnetization does not relax fully between scans through the signal. When this occurs the B_1 required for maximum signal amplitude depends on scan frequency as well as on scan rate.

For the scan rates and widths used in these studies, the z-axis magnetization does not fully relax between successive traverses of the signal for scan rates faster than about 3.2×10^4 G/s. When relaxation is not complete, the steady-state signal amplitude for the same scan rate is strongly dependent on scan width, because that determines the fraction of the scan time that the signal is on resonance, and on B_1 because that determines the energy deposited in the spin system during each traverse. Because data were collected at various combinations of scan width and scan frequency, the data in Figs. 6 and 7 are not smooth functions of scan rate. The points that were used to generate the solid lines in Figs. 6 and 7 were calculated for the experimental scan widths and frequencies so the calculated lines also are not smooth functions of scan rate.

The relative signal amplitudes of the trityl-CD_3 signal as a function of scan rate are shown in Fig. 6. At a constant B_1 of 4.6×10^{-3} G the signal intensity decreases as the scan rate increases above about 3×10^3 G/s due to decreasing energy deposition in the signal. This B_1 is only a factor of two below that required for maximum signal amplitude at the slowest scans studied, so the initial change in signal amplitude with increasing scan rate is relatively small. The peak intensity as a function of scan rate occurs at much lower scan rate for the trityl-CD_3 signal (Fig. 6) than for the LiPc signal (Fig. 2) because of the longer relaxation times for trityl-CD_3 than for LiPc. The calculations of signal intensities as a function of scan rate were performed for combinations of scan width and scan frequency similar to ones used in the experiments. For the same scan rate substantially higher values of relative signal intensity are predicted for wider scans with lower scan frequency because of the smaller fraction of time that the signal is on resonance. Because of the shorter relaxation times for LiPc than for trityl-CD_3, the RF B_1 values required to obtain the maximum signal amplitude are higher for LiPc (Fig. 3) than for trityl-CD_3 (Fig. 7).

The spectra shown in Fig. 4A were obtained at B_1 values that are a factor of two less than the values for maximum signal amplitude. At these B_1 values the signal amplitude is about 85% of the maximum value and the linewidths are within experimental uncertainty of the ones observed in the regime where signal increases linearly with B_1. At the B_1 that gave the maximum signal amplitude, the linewidths were about 10% greater than in the linear response regime. Thus, just as in slow scans, there is a trade-off between higher signal amplitude and line broadening as RF B_1 is increased.

4. Discussion

The spectra shown in Figs. 1A and 4A demonstrate the impact of rapid scans on the EPR lineshapes for signals centered in the scans. A signal that is offset from the center would be subject to a slower scan rate and the oscillations would be less deep. The x-axes in the plots of signal amplitude and B_1 required to achieve maximum signal amplitude (Figs. 2, 3, 6, and 7) refer to the scan rate as the field traverses the resonance condition. For a signal at the center of the scan the scan rate is maximum and the amplitude, lineshape, and B_1 for maximum amplitude depend only on the product of scan frequency × scans width, provided that the spins relax fully between the times that the magnetic field passes through resonance. At positions in the scan other than the center the sinusoidal magnetic field scans cause the relationship between time and magnetic field to depend on scan width and scan frequency, independently, rather than simply on the product of the two variables. Thus, for the scans at 3.3×10^5 G/s which were obtained with 50 kHz scan frequency and 2.1 G scan width the oscillations in the extremes of the scans are different than would be obtained for a scan rate of 3.3×10^5 G/s at 25 kHz with a scan width of 4.2 G even though the shapes and intensities in the centers of the scans would be superimposable.

To provide perspective on the rapid-scan experiments, the calculated curves in Figs. 6 and 7 extend to slower scan rates than were experimentally accessible with the spectrometer used. For the relaxation times of

trityl-CD_3 the signal amplitude at constant B_1, the maximum signal amplitude as a function of RF B_1, and the B_1 required to achieve the maximum signal amplitude are independent of scan rate at rates less than about 100 G/s. These are the characteristics of the slow-scan regime. The maximum amplitude of the trityl signal was observed at a scan rate of about 2×10^4 G/s and the signal amplitude was about a factor of three greater than in the slow-scan regime. At this scan rate the broadening of the line is less than a factor of two, which suggests that it will be possible to deconvolute the distortion and restore the undistorted lineshapes, as has been done in NMR [6]. The plots in Figs. 2 and 6 illustrate the enhancement in signal amplitude that can be achieved at constant numbers of scans when operating at B_1 near that which gives the maximum signal amplitude. In the same amount of time, many more averages can be performed at the faster scan rate, which provides the opportunity for substantial enhancement in digitally accumulated signal amplitude per unit time.

For EPR imaging rapid-scan experiments may have two major advantages compared with pulsed experiments. The rapid decay of the FID in the presence of a magnetic field gradient limits EPR imaging gradients to very small values [31]. With small magnetic field gradients across the sample the long relaxation times characteristic of the trityl radicals result in electron spin echoes that are very broad, which provides a substantial challenge for imaging based on echoes. The rapid-scan spectra may avoid both of these problems while still permitting rapid signal acquisition and require substantially less source power than the pulse experiments. Rapid scans also may be useful for species for which T_2 is too short to observe echoes or FIDs.

Acknowledgments

Financial support from National Institute of Health NIBIB EB000557 is gratefully acknowledged. Professor Harold Swartz, Dartmouth University, graciously provided the LiPc which was prepared with funding from NIBIB EB002180. The trityl-CD_3 radical was a generous gift from Nycomed Innovations AB to Professor Howard Halpern, University of Chicago, who supplied it for this study, as a collaborative project under NIBIB EB002034. We thank Janusz Koscielniak (National Cancer Institute) for bringing [20] to our attention and to him and to Martyna Elas (Jagiellonian Institute, Krakow, Poland) for assistance in its translation.

References

[1] N. Bloembergen, E.M. Purcell, R.V. Pound, Phys. Rev. 73 (1948) 679–712.
[2] B.A. Jacobsohn, R.K. Wangness, Phys. Rev. 73 (1948) 942.
[3] J.I. Kaplan, J. Chem. Phys. 57 (1972) 5615–5616.
[4] J.I. Kaplan, J. Chem. Phys. 59 (1973) 990.
[5] R.R. Ernst, J. Chem. Phys. 59 (1973) 989.
[6] J. Dadok, R.F. Sprecher, J. Magn. Reson. 13 (1974) 243–248.
[7] R.K. Gupta, J.A. Ferretti, E.D. Becker, J. Magn. Reson. 13 (1974) 275–290.
[8] R.K. Gupta, J.A. Ferretti, E.D. Becker, J. Magn. Reson. 16 (1974) 505–507.
[9] D. Shaw, Specialist Periodical Reports, Nuclear Magn. Reson. 5 (1976) 188–204.
[10] F. Bloch, Phys. Rev. 70 (1946) 460–474.
[11] A.M. Portis, Phys. Rev. 100 (1955) 1219–1221.
[12] M. Weger, Bell Syst. Tech. J. 39 (1960) 1013–1112.
[13] J.S. Hyde, Phys. Rev. 119 (1960) 1483–1492.
[14] J.S. Hyde, L. Dalton, Chem. Phys. Lett. 16 (1972) 568–572.
[15] C. Mailer, C.P.S. Taylor, Biochim. Biophys. Acta 322 (1973) 195–203.
[16] A. Abragam, B. Bleaney, Electron Paramagnetic Resonance of Transition Ions, Oxford University Press, Oxford, 1970.
[17] J.S. Hyde, Methods in Enzymology XLIX (1978) 480–511.
[18] J.S. Hyde, L.R. Dalton, in: L.J. Berliner (Ed.), Spin Labeling II, Academic Press, New York, 1979, pp. 1–70.
[19] S.K. Rengan, V.R. Bhagat, V.S.S. Sastry, B. Venkataraman, J. Magn. Reson. 33 (1979) 227–240.
[20] R. Czoch, J. Duchiewicz, A. Francik, S. Indyka, J. Koscielniak, Meas. Automatic Control 29 (1983) 41–43.
[21] J.F. Dunn, H.M. Swartz, Methods 30 (2003) 159–166.
[22] J.H. Ardenjaer-Larsen, I. Laursen, I. Leunbach, G. Ehnholm, L.-G. Wistrand, J.S. Petersson, K. Golman, J. Magn. Reson. 133 (1998) 1–12.
[23] P. Turek, J.J. Andre, A. Giraudeau, J. Simon, Chem. Phys. Lett. 134 (1987) 471–476.
[24] V.O. Grinberg, A.I. Smirnov, O.Y. Grinberg, S.A. Grinberg, J.A. O'Hara, H.M. Swartz, Appl. Magn. Reson. (2004) in press.
[25] R.W. Quine, G.A. Rinard, S.S. Eaton, G.R. Eaton, Magn. Reson. Eng. 15 (2002) 59–91.
[26] J.R. Harbridge, G.A. Rinard, R.W. Quine, S.S. Eaton, G.R. Eaton, J. Magn. Reson. 156 (2002) 41–51.
[27] W.H. Press, S.A. Teukolsky, W.T. Verrling, B.P. Flannery, Numerical Recipes in Fortran: The Art of Scientific Computing, Cambridge University Press, Cambridge, UK, 1992, pp. 704–708.
[28] G.K. Wertheim, M.A. Butler, K.W. West, D.N.E. Buchanan, Rev. Sci. Instrum. 45 (1974) 1369–1371.
[29] L. Yong, J. Harbridge, R.W. Quine, G.A. Rinard, S.S. Eaton, G.R. Eaton, C. Mailer, E. Barth, H.J. Halpern, J. Magn. Reson. 152 (2001) 156–161.
[30] J. Weil, J.R. Bolton, J.E. Wertz, Electron Paramagnetic Resonance: Elementary Theory and Practical Applications, Wiley-Interscience, New York, 1994, pp. 493–494.
[31] S. Subramanian, N. Devasahayam, K. Yamada, J. Cook, A. Taube, J.B. Mitchell, J.A.B. Lohman, M.C. Krishna, Magn. Reson. Med. 48 (2002) 370–379.